Journal of Catalysis **203,** 133–149 (2001)
doi:10.1006/jcat.2001.3322, available online at http://www.idealibrary.com on IDEAL®

Redox Behavior of Copper Oxide/Zinc Oxide Catalysts in the Steam Reforming of Methanol Studied by *in Situ* X-Ray Diffraction and Absorption Spectroscopy

M. M. Günter, T. Ressler,[1] R. E. Jentoft, and B. Bems

Department of Inorganic Chemistry, Fritz-Haber-Institut der Max-Planck-Gesellschaft, Faradayweg 4-6, D-14195 Berlin, Germany

Received February 21, 2001; revised June 13, 2001; accepted June 27, 2001

The bulk structure of copper in various binary Cu/ZnO catalysts for steam reforming of methanol under activation and working conditions is studied by *in situ* X-ray diffraction (XRD) and X-ray absorption spectroscopy (XAS). The evolution of bulk phases from CuO/ZnO precursors during activation with hydrogen was studied using temperature-programmed reduction (TPR) (448–523 K, 2 vol% H_2 with and without water vapor). With decreasing copper content the onset of reduction is shifted from 473 K (pure CuO) to 443 K (40 mol% Cu) accompanied by a decrease in Cu crystallite sizes (from 210 Å to 40 Å). Using time-resolved *in situ* XANES measurements at the Cu K-edge during TPR experiments the degree of reduction was monitored. It is shown that Cu(I) oxide forms prior to Cu. Adding oxygen to the feed gas leads to the formation of a mixture of Cu(II) and Cu(I) oxide accompanied by a complete loss of activity. After switching back to steam reforming conditions a higher activity is attained while the catalyst shows an increased Cu crystallite size (up to 40%). EXAFS measurements at the Cu K-edge and the Zn K-edge indicate a structural disorder of the Cu particles in the medium range order based on increasing Debye–Waller factors for higher Cu–Cu shells. Furthermore, the dissolution of Zn atoms (up to ~4 mol%) in the copper lattice is detected. Upon oxidation/reduction cycles activity is increased, the disorder in the copper particles increases, and Zn segregates out of the copper bulk. A structural model is proposed which ascribes the enhanced activity to structurally disordered (strained) copper particles due to an improved interface interaction with ZnO.

Key Words: **Cu/ZnO catalysts; methanol steam reforming; temperature-programmed reduction; XRD; XANES; *in situ*; phase evolution; structure; selectivity; activity; XAFS.**

INTRODUCTION

Cu/ZnO catalysts can be used to produce hydrogen by steam reforming of methanol with high selectivity and activity (1, 2). Thus, methanol often is considered as an alternative "automotive" fuel and could serve as a potential hydrogen source for fuel cell applications (3). Current efforts are dedicated to the minimization of selectivity to CO which acts as a poison in fuel cell applications (4). The steam reforming reaction ($CH_3OH + H_2O \rightarrow CO_2 + 3H_2$) can be regarded as the reversed methanol synthesis reaction. However, a detailed reaction mechanism is still under debate (5–7). In a kinetic model by Peppley *et al.* it is assumed that different active phases are responsible for the methanol decomposition, methanol steam reforming, and the water–gas shift reaction (8).

The Cu/ZnO system has been studied extensively after reduction and under working conditions of methanol synthesis (9–11 and references cited therein). However, the active Cu phase for methanol reforming is not fully elucidated yet. Previously, differences in the reduction kinetics of CuO/ZnO were mainly studied by conventional temperature-programmed reduction (TPR) methods (12, 13). However, these methods do not measure the structural evolution of the catalyst during reduction (e.g., evolution of different bulk phases). Fierro *et al.* studied the reduction of CuO/ZnO with different Cu/Zn ratios and found a promoting effect of ZnO on the reducibility of CuO (14). The reduction kinetics of copper oxide were determined by thermogravimetric methods (15, 16) which afforded sigmoidal curves indicating a nucleation growth mechanism. Structural investigations of the copper phase under reduction conditions based on XRD have been reported by Himelfarb *et al.* (17) and Vong *et al.* (18). Himelfarb *et al.* and Porta *et al.* (19) described an intermediary Cu_2O phase, whereas this phase was not observed by Vong *et al.* However, the detection of Cu_2O is based on *ex situ* investigations which may not represent the "real" state of the Cu phase under reduction conditions. Als-Nielsen *et al.* reported on an *in situ* detection of Cu_2O by time-resolved QEXAFS without further analyzing the growth kinetics of this phase (20). Reitz *et al.* (21) observed Cu^+ as a transient species in the reduction of CuO/ZnO catalysts by time-resolved XANES. Fernández-García *et al.*

[1] To whom correspondence should be addressed. Fax: (+49) 30 8413 4405. E-mail: ressler@fhi-berlin.mpg.de.

0021-9517/01 $35.00

reported on the basis of a statistical analysis of TPR data of Cu/Al_2O_3 that the reduction process of copper aluminate proceeds via a two-step mechanism (22). Recently, Grunwaldt *et al.* observed dynamical changes of the Cu coordination number upon changes in the gas-phase reduction potential by *in situ* EXAFS during methanol synthesis (23).

Regarding the active state of Cu/ZnO catalysts, different authors claim that the ratio of Cu/Cu^+ governs the methanol conversion (24). This interpretation is closely related to the model of the active Cu/ZnO phase in methanol synthesis developed by Klier (25). Peppley *et al.* on the basis of a surface mechanism for methanol steam reforming proposed in a recent publication that the nature of the active sites differs according to their function (8), but no structural details are provided. The effects of the preparation conditions of precursors for Cu/ZnO catalysts upon precursor phases, surface structure, and catalytic activity for steam reforming of methanol has been investigated by Shen *et al.* (26).

In this study we used two complementary bulk techniques, *in situ* X-ray diffraction and X-ray absorption spectroscopy to elucidate bulk structural changes of Cu in Cu/ZnO systems during activation and under methanol steam reforming conditions. First, the evolution of bulk phases during activation of the catalyst (i.e., reduction in hydrogen with ("wet") and without ("dry") additional water vapor) was investigated. Second, correlations between the bulk structure of Cu on ZnO and activity or selectivity in the steam reforming of methanol are presented.

EXPERIMENTAL PROCEDURE

CuO/ZnO Preparation and Characterization

CuO/ZnO precursors were prepared according to the coprecipitation method, both at a constant pH of 7.0 and with decreasing pH, from metal nitrate and sodium carbonate solutions. Binary hydroxycarbonate precursors of a systematic series with varying Cu/Zn molar ratios were obtained and are denoted in the following according to their nominal Cu/Zn atomic ratio (100/0, 90/10, 80/20, 70/30, 60/40, 50/50, 40/60, 30/70, 20/80, 10/90, 0/100). Calcination of the hydroxycarbonate precursors at 600 K for 3 h in a muffle furnace in air afforded mixed CuO/ZnO systems. More preparative details are given elsewhere (27).

Specific surface areas were calculated by applying the BET method to the nitrogen isotherms obtained at liquid nitrogen temperature on samples outgassed at 423 K using a Quantasorp Jr. (Quantachrom) adsorption instrument.

The sample nomenclature including the pH of the preparation and characterization of the calcined precursor with respect to CuO and ZnO crystallite size and the BET surface area is given in Table 1.

TABLE 1

Chemical Composition and Characterization of Calcined CuO/ZnO Precursors and Reduced Cu/ZnO

Sample name	Nominal Cu/Zn ratio (atom%)	Chemical composition[a] Cu/Zn (atom%)	pH during precipitation	CuO crystallite[b] size (Å)	ZnO crystallite size (Å)	S_{BET} (m^2/g)	Onset of reduction (K)		Cu crystallite size[e] (Å)	
							"dry"[f]	"wet"[g]	"dry"	"wet"
C100/0	100/0	100/0	Constant (7.0)	137	—	33	463	468	215	190
C90/10	90/10	91/09	Constant (7.0)	59	—[c]	70	443	458	112	127
C80/20	80/20	82/18	Constant (7.0)	41	—[c]	76	473	443	90	92
C70/30	70/30	73/27	Constant (7.0)	40	40	76	438	458	68	70
C60/40	60/40	63/37	Constant (7.0)	46	43	82	443	453	77	78
C50/50	50/50	53/47	Constant (7.0)	46	43	89	463	453	50	58
C40/60	40/60	45/55	Constant (7.0)	45	46	96	443	448	42	47
D100/0	100/0	100/0	Decreasing	125	—	45	458	468	148	171
D70/30	70/30	74/26	Decreasing	100	71	83	448	463 ± 5[d]	81	79
D60/40	60/40	66/34	Decreasing	78	66	89	448	453	101	108
D50/50	50/50	56/44	Decreasing	58	64	96	448	468	45	52
D40/60	40/60	46/54	Decreasing	60	77	99	443	453	38	40

Calcination conditions: 600 K for 3 h in stagnant air. Onset of reduction during TPR and the corresponding copper crystallites sizes after reduction are measured by *in situ* XRD. The reduction was performed under both "dry" and "wet" reducing conditions.

[a] Cu/Zn ratio determined by X-ray absorption.

[b] Calculated using the Scherrer equation for CuO (111) and ZnO (100).

[c] Not determined because of poor crystallinity.

[d] Reproduced in three measurements.

[e] Determined at the end of the TPR run at 523 K.

[f] Reduction performed in ~2 vol% H_2.

[g] Reduction performed in ~2.5 vol% H_2 and 3 vol% H_2O.

In Situ XRD

The *in situ* XRD experiments were conducted using a STOE STADIP P diffractometer (Cu $K\alpha$ radiation) in the Bragg–Brentano scattering geometry equipped with a secondary monochromator and a scintillation counter operated in the stepping mode. The *in situ* cell consisted of a Bühler HDK S1 high-temperature diffraction chamber mounted onto the goniometer (28). In addition to a gas feed system for He, O_2, and H_2 as described in Ref. (28), H_2O and MeOH were introduced by saturation of He with the respective liquids. Typically, 12 mg of the catalyst sample was used. Prior to any experiment the reactor was purged with He. Reduction of the precursors was performed *in situ* following a temperature program and in either 2 vol% H_2 (denoted in the following as "dry" reduction) or in 2.5 vol% H_2 and 3 vol% H_2O ("wet" reduction) both in a He flow of 100 ml/min. During precursor reduction and at temperatures between 433 K and 523 K an XRD pattern was recorded every 5 K at a constant temperature while applying a temperature ramp between every measurement resulting in an effective temperature ramp of 0.5 K/min. Thus, the uncertainty in onset temperatures of reduction is 5 K. For the measurements during temperature-programmed reduction a counting time of 2 s/step and a step width of 0.04° 2θ was chosen for an interval of 41–46° 2θ. The gas phase over the sample was analyzed quantitatively on-line with a Balzers Prisma 200 quadrupole mass spectrometer.

The full width at half-maximum (FWHM) and integrated intensity of XRD lines were determined by fitting pseudo-Voigt (fixed Gauss contribution) and Lorentz profile functions (more appropriate for strongly broadened profiles) to the Cu (111) peak. The Scherrer formula was used to estimate the crystallite size on the basis of the FWHM without taking other broadening effects and correction for instrumental broadening into account (29). Calculation of theoretical X-ray powder patterns and lattice constant refinements were done using the software PowderCell v2.2 (30).

In Situ X-Ray Absorption Spectroscopy

The *in situ* XAS experiments were performed at beam line X1 at the Hamburger Synchrotron Radiation Laboratory, HASYLAB, using a Si(111) double-crystal monochromator. The storage ring was operated at 3.6 GeV with injection currents of 150 mA.

The *in situ* XAS experiments were carried out in the transmission mode in a flow reactor at atmospheric pressures (31). CuO/ZnO samples prepared according to both preparation methods were investigated (constant pH samples C70/30, C60/40, C40/60, C30/70, C10/90 and decreasing pH samples D70/30, D60/40, D40/60). The samples were mixed with boron nitride (mass ratio CuO/ZnO : BN = 1 : 6) and 45 mg of the mixture was pressed with a force of one ton into a 5-mm-diameter pellet. The absorption jump at the Cu K-edge was ~1.5. XANES spectra were measured in the Quick-EXAFS mode with a time resolution of 15 s/spectrum (8959–9100 eV).

A calibrated mass spectrometer (QMS200 Pfeiffer) permitted a quantitative analysis of the gas phase during the experiments. *In situ* EXAFS spectra were measured after oxidation and re-reduction to reveal structural changes of the Cu and Zn phases present. Temperature-programmed reduction (TPR) runs were performed with 2 vol% H_2 (constant pH samples) and 8 vol% H_2 (decreasing pH samples) from 448–523 K with a temperature ramp of 5 K/min.

XANES and EXAFS Data Analysis

The software WinXAS v2.0 (32) was used for an analysis of the time-resolved Cu K-edge XANES data to reveal qualitative and quantitative information on the copper bulk phases under TPR and steam reforming conditions. Identification of the number of phases was achieved by principal component analysis (PCA) of the experimental XANES spectra. Reference spectra of these phases were then used in a least-squares fitting procedure of the time-resolved spectra to determine the fraction of each phase present (33). For the extended absorption fine structure (EXAFS) analysis, a smooth atomic background, $\mu_0(k)$, was obtained using cubic splines. The radial distribution function FT($\chi(k)$) was obtained by Fourier-transforming the k^3-weighted experimental $\chi(k)$ function, multiplied by a Bessel window, into R space. EXAFS data analysis was carried out using theoretical backscattering phases and amplitudes calculated with the *ab initio* multiple-scattering code FEFF 7(34). Single-scattering and multiple-scattering paths in the employed model structures were calculated up to 6 Å for Cu metal and up to 5 Å for ZnO with a lower limit of 2.0% in amplitude with respect to the strongest backscattering path. In addition to the Zn–O and Zn–Zn distances extra Zn–Cu shells were employed assuming Zn on Cu sites in fcc Cu metal. EXAFS fitting and simulation were performed using the standard EXAFS formula (k range from 2.0 to 13 $Å^{-1}$, R range 1.5 to 6.0 Å (35). Structural parameters that are determined by a least-squares EXAFS fit to experimental spectra are (i) one E_0 shift for all scattering paths in the Cu bulk structure, (ii) Debye–Waller factors for single-scattering paths, (iii) single scattering shell distances, R_i, and (iv) a third cumulant (36) to account for slight deviations from a Gaussian pair distribution function. Coordination numbers (CN) were kept constant in the refinement. This restriction was necessary to reduce the number of free running parameter (N_{free}) to much less than the number of independent parameters (N_{ind}) in the experimental data used. EXAFS refinements reported here were carried out in R space to fit the magnitude and imaginary part of a Fourier-transformed k^3-weighted experimental $\chi(k)$. More details about the XAFS fitting procedure employed can be found in Ref. (37).

In Situ Methanol Steam Reforming Activity

The catalytic activity of the Cu/ZnO samples for steam reforming of methanol was determined at atmospheric pressure and 523 K using saturators for methanol and water at room temperature. After temperature-programmed reduction and cooling to 298 K, the binary Cu/ZnO samples were exposed to $MeOH/H_2O$ vapor in a ratio of 4/1 ($c(MeOH) \sim 6$ vol%, $c(H_2O) \sim 1.5$ vol%) diluted in He; total flow through the XRD cell was 120 ml/min, and through the XAS cell was 25 ml/min. Next, the temperature was increased from RT to 523 K at 20 K/min. Reactants and products (MeOH, H_2O, H_2, CO_2, and CO) were quantitatively monitored with a mass spectrometer (time resolution 12 s/scan). In order to measure changes in the phase composition during oxidation and reduction cycles, oxygen was added to the feed at 523 K while the reaction was progressing (22 vol% O_2 for intervals of 100 min (*in situ* XRD) and 15 vol% O_2 for 10 min (*in situ* XAS)).

In the following, selectivity refers to CO_2 instead of H_2 because reactions other than the desired steam reforming produce hydrogen as well (i.e., decomposition to carbon monoxide and hydrogen, and dehydrogenation to formaldehyde and hydrogen). In addition, the water–gas shift reaction may also produce hydrogen. An error is introduced by not differentiating the CO_2 stemming from the water–gas shift reaction. However, this reaction occurs to a much smaller extent than the steam reforming reaction.

In order to express the hydrogen production activity in terms of a turnover frequency (i.e., number of product molecules of hydrogen formed per surface atom Cu per second) the number of exposed Cu surface atoms must be estimated. The number of surface atoms was calculated for the Cu surface area using a mean surface atom density of 1.47×10^{19} m^{-2} (38). The copper surface area was determined using the XRD crystallite size and assuming a spherical copper crystallite shape. The assumption of spherical copper particles is based on crystallite sizes estimated from the Cu (200) peak for samples with high copper concentration (>60 mol% Cu) which yielded values similar to those derived from the Cu (111) peak. We have previously shown that the Cu surface area thus determined agrees well with the surface area based on chemical titration with N_2O (39).

RESULTS

(I) In Situ XRD

(a) Reduction of the CuO/ZnO precursor. Structural changes of the CuO/ZnO system were monitored by *in situ* XRD during temperature-programmed reduction (TPR). The evolution of the intensity of the Cu (111) line afforded the onset and extent of reduction while the evolution of the crystallite size was obtained from the line width. In Fig. 1 the normalized H_2 and H_2O MS signals are correlated to the intensity evolution of the Cu (111) peak during TPR of the sample D70/30 in the range from 433 K to 523 K in 2 vol% hydrogen. It can be seen that the uptake of H_2 coincides with the evolution of H_2O. The increase in the intensity of the Cu (111) peak indicates the growth of Cu crystallites. Because Cu particles large enough to be detected by XRD need to form, the onset of the evolution of the Cu (111) line is delayed with respect to the hydrogen uptake and the evolution of water.

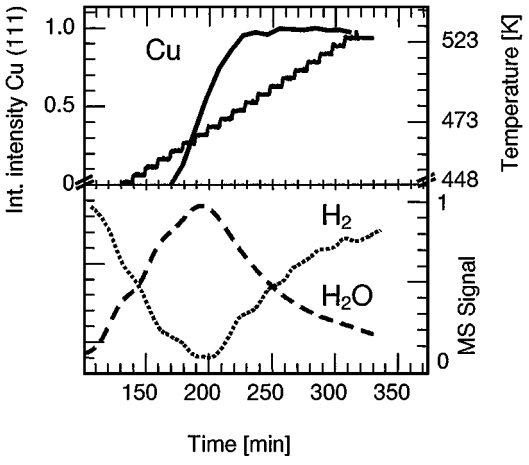

FIG. 1. Evolution of integrated intensity of the Cu (111) peak and normalized mass spectrometer signals of H_2O and H_2 during TPR of CuO/ZnO sample (D70/30) in 2 vol% hydrogen measured by *in situ* XRD. Measuring time 7 min/scan with an effective temperature ramp of 0.5 K/min.

Results of the TPR of all samples are summarized in Table 1. In most cases the onset temperature of "wet" reduction was about 10 K higher than the onset temperature of "dry" reduction. For the constant pH preparation and "wet" reduction conditions decreasing copper content leads to a lower onset of reduction temperature; from 468 K (pure CuO, sample C100/0) to 448 K (sample C40/60), with sample C80/20 being an exception to this trend. For the decreasing pH samples a similar trend of decreasing onset temperature with decreasing Cu content is apparent for both "dry" and "wet" reduction conditions, with sample D50/50 under "wet" reduction conditions being an exception to this trend. No similar trend is apparent for the samples from the constant pH preparation under "dry" reduction conditions. In addition, in most cases, "wet" reduction leads to an increase in Cu crystallite size with respect to that of "dry" reduction (average increase ~4 Å). With increasing Zn content the Cu/ZnO samples exhibited a decreasing Cu crystallite size. The exceptions to the trend of decreasing Cu particle size with increasing Zn content are the 60/40 samples.

The evolution of the Cu crystallite size during TPR is shown in Fig. 2 as a function of the temperature. The Cu crystallite size appears to increase linearly with time

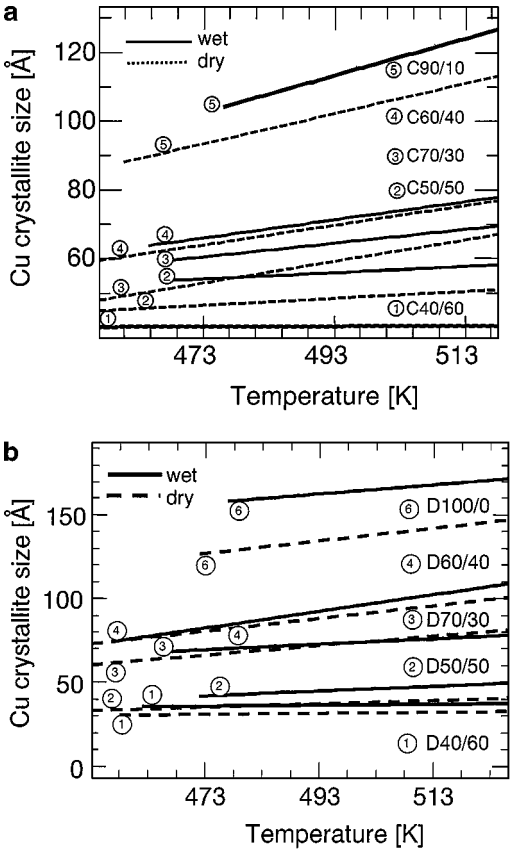

FIG. 2. Evolution of Cu crystallite size during TPR for samples with different Cu/Zn ratios measured both in 3 vol% H_2 ("dry") and 2.5 vol% H_2 + 3 vol% H_2O ("wet") in 100 ml/min He for both sets of sample preparations: (a) constant pH preparation, (b) decreasing pH preparation. The temperature was raised with an effective temperature ramp of 0.5 K/min.

(applying an effective temperature ramp of 0.5 K/min). For samples with lower Cu concentrations the difference in crystallite size for "wet" and "dry" reduced samples is much less pronounced than for Cu-rich samples.

(b) Steam reforming of methanol. The characteristics of the catalytic activity of Cu/ZnO catalysts obtained from both preparation batches and reduction procedures ("dry" and "wet") are summarized in Table 2. Highest conversion (38%) is obtained for the "wet" reduced sample D70/30, whereas the "wet" reduced copper-rich sample D100/0 exhibits the lowest conversion. Similarly, the selectivity shows a strong dependence on the composition and reduction conditions and ranges from 79% ("wet" C60/40) to 16% ("dry" C90/10). The "wet" reduced samples C60/40, C50/50, and C40/60 and D60/40, D50/50, and D40/60 show the same sequence in selectivity (i.e., S_{CO_2}, 60/40 > S_{CO_2}, 50/50 > S_{CO_2}, 40/60) with similar absolute values (see Table 2). While selectivity to CO_2 is a function of conversion for all samples, at the same level of conversion the "wet" reduced samples exhibit an enhanced selectivity compared to that of the "dry" reduced samples. Selectivities of the "dry" reduced samples are between 10 and 40% lower than those of the "wet" reduced samples. Highest selectivities to CO_2 of ~80% at ~20% conversion are obtained for the "wet" reduced samples C70/30 and C60/40 (see Table 2).

The *in situ* XRD investigations allowed calculation of the Cu crystallite sizes of *operating catalysts* which can be used to estimate copper surface areas. Hence, it is possible to detect influences of the Cu crystallite size (and metal surface area) on the activity without transferring the sample for *ex situ* measurements.

The Cu crystallite sizes measured during the steam reforming of methanol, and determined from the Cu (111) line width, are presented in Table 2. It can be seen by comparison with the crystallite sizes presented in Table 1, measured at the end of the precursor reduction, that during reaction the crystallite sizes increase. Furthermore, the same relationship of decreasing crystallite sizes with decreasing Cu content is obtained; however, in some cases the initially larger "wet" reduced crystallites do not increase in size as much as the "dry" reduced samples and so during reaction exhibit a smaller crystallite size (e.g., samples C80/20, C60/40, C70/30) than the "dry" reduced samples.

It can be seen from Table 2 that the D-series samples exhibit a higher hydrogen production rate than the samples of the C-series. Furthermore, the samples prepared at constant pH show a greater variation in H_2 production rate than the D-series samples of similar Cu surface area.

The TOF for the initial activity as a function of ZnO content in the catalysts is given in Fig. 3. The reaction rate is normalized to the number of Cu metal surface atoms. It can be seen that the TOF values vary with the catalyst composition having maximum values of 0.80 s^{-1} for the "dry" reduced sample C60/40 and of 1.47 s^{-1} for the "wet" reduced sample D60/40. In addition, samples prepared at decreasing

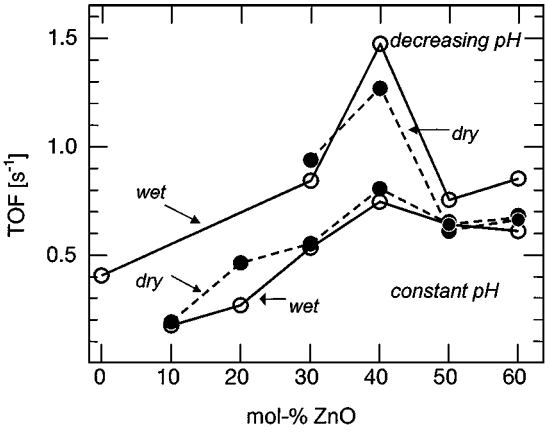

FIG. 3. Initial turnover frequency (TOF) for hydrogen production as a function of ZnO content for catalysts prepared according to the decreasing or the constant pH method (both under "dry" and "wet" reduction conditions). Reaction conditions: $MeOH/H_2O = 4/1$, $p = 101$ kPa, total flow ~140 ml/min.

TABLE 2

Initial Methanol Steam Reforming Catalytic Activity Data (Conversion of Methanol, Selectivity to CO_2, Hydrogen Production Rate) and Corresponding Cu Crystallite Size Determined by *in Situ* XRD

Sample	Reduction conditions	Cu crystallite size (Å)	Conversion of MeOH X_{MeOH} (%)	Selectivity to CO_2, S_{CO_2} (%)	Hydrogen production rate, r_{H_2} (μmol $H_2 \cdot g_{cat}^{-1} \cdot s^{-1}$)	Cu surface area[a] $S_{Cu(XRD)}$ ($m^2 \cdot g^{-1}$)	TOF[b] (s^{-1})
C100/0	Dry	250	No activity	No activity		13.6	—
	Wet	210	—	—		16.0	—
C90/10	Dry	151	14	16	92	20.2	0.19
	Wet	163	15	17	77	18.1	0.17
C80/20	Dry	123	26	34	245	22.2	0.46
	Wet	110	13	0	145	23.2	0.27
C70/30	Dry	95	24	60	333	25.5	0.55
	Wet	86	22	78	293	22.2	0.54
C60/40	Dry	96	36	39	350	18.1	0.80
	Wet	95	20	79	318	19.5	0.74
C50/50	Dry	61	29	56	380	24.6	0.64
	Wet	64	20	72	349	22.2	0.64
C40/60	Dry	48	22	50	385	23.9	0.67
	Wet	56	27	56	318	20.9	0.61
D100/0	Dry	250	—[c]	—[c]		12.9	—
	Wet	247	10	29	131	13.2	0.41
D70/30	Dry	101	33	42	485	21.1	0.94
	Wet	104	38	37	426	20.7	0.84
D60/40	Dry	113	32	43	482	15.5	1.27
	Wet	137	23	72	480	13.3	1.47
D50/50	Dry	56	19	50	402	26.8	0.61
	Wet	59	20	67	460	25.0	0.75
D40/60	Dry	42	29	53	433	26.7	0.66
	Wet	51	27	59	480	23.0	0.85

Reaction conditions: $MeOH/H_2O = 4/1$, $p = 101$ kPa, total flow ~140 ml/min.

[a] Calculated from the Cu crystallite size based on XRD data obtained during reaction.

[b] Hydrogen molecules produced per surface copper atom per second.

[c] Fast deactivation.

pH show a higher TOF than the samples of the constant pH series. The differences in the TOF for "wet" reduced samples as compared to that of those which underwent "dry" reduction are small.

(c) Oxygen addition cycle. In Fig. 4 four XRD patterns of a Cu/ZnO catalyst (sample C60/40) obtained after calcination (a), steam reforming (b), oxidation (c), and re-reduction (d) are displayed. The pattern indicative of CuO (a) is converted to that of metallic Cu (b) after the calcined sample is reduced in the steam reforming feed with no additional copper oxide phases detectable. The addition of 22 vol% O_2 to the feed at 523 K for 100 min resulted in the formation of mostly Cu(I) oxide together with some minor amounts of Cu(II) oxide (c). After re-reduction in the feed at 523 K the XRD pattern of metallic Cu can be seen, but with a decreased line width of the Cu (111) peak (d). Changes in the product gas-phase composition (H_2, MeOH, CO_2, and H_2O) during two oxygen addition cycles are depicted in Fig. 5. It can be seen that adding oxygen to the feed resulted in a complete loss of activity for the steam reforming reaction. In addition, the formation of water and CO_2 during the oxygen addition indicates the occurrence of total

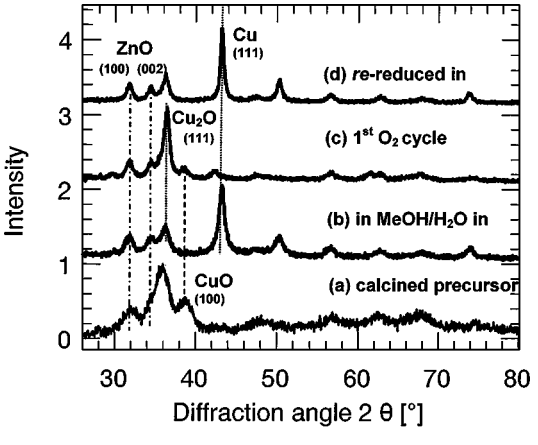

FIG. 4. X-ray diffraction patterns of a sample with a composition of 60 atom% Cu and 40 atom% Zn (C60/40) during different stages of treatment. Upon reduction the calcined CuO (a) is transformed into Cu metal which is preserved under methanol steam reforming conditions at 523 K (b). Oxygen treatment resulted in a mixture of Cu(I) oxide and Cu(II) oxide (c). The oxidic copper phases are re-reduced in the feed to metallic Cu with a decreased line width (d). Characteristic (*hkl*) diffraction lines of CuO, Cu_2O, and Cu metal are indicated.

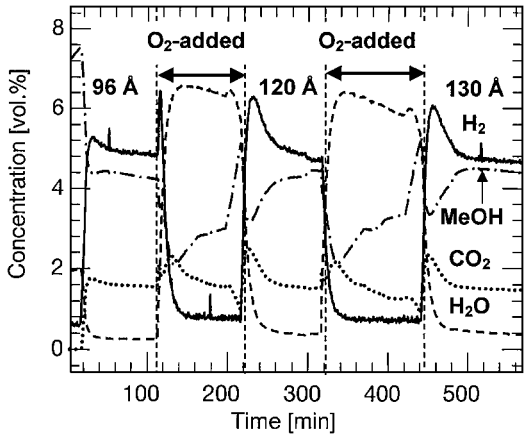

FIG. 5. Evolution of gas-phase concentration of H_2, MeOH, CO_2, and H_2O in XRD cell under methanol steam reforming conditions during addition of oxygen (15 vol% O_2) to the feed for two intervals of ~100 min. Sample C60/40 "dry" was used. The change of Cu crystallite size is also indicated.

oxidation of methanol. The low hydrogen concentration observed during oxygen addition intervals might result from methanol dehydrogenation. The oxidative poisoning was, however, completely reversible with no loss in hydrogen productivity. Oxidation and re-reduction experiments were carried out on selected samples (C70/30, C60/40, C40/60) activated under "dry" reduction conditions. The copper crystallite sizes, the methanol conversion, and the selectivity are summarized in Table 3. An increase in conversion, selectivity, and hydrogen production rate with extending number of oxidation/reduction cycles is observed. In addition, the copper crystallite size expands with each oxidation cycle (Table 3). For example, the copper crystallite size of the sample C70/30 increases from 76 to 110 Å and then to 120 Å. After the oxidation/reduction cycles the XRD peaks of ZnO (e.g., (100), (002)) are similarly affected in that their profiles become gradually more pronounced. Profile fitting of the ZnO (100) peak of C70/30 sample gives crystallite sizes that increase slightly upon oxidation and re-reduction from 80 to 90 Å. The relative changes of the copper and zinc oxide lattice parameter after reduction, under stream reforming conditions, and after successive oxygen/re-reduction cycles are depicted in Fig. 6. The continuous increase in lattice parameter of Cu and ZnO indicates an expansion of the unit cell under methanol steam reforming conditions after each oxidation/re-reduction step with respect to the freshly reduced sample.

(II) In Situ XAFS

(a) Reduction of CuO/ZnO precursor. *In situ* X-ray absorption spectroscopy was performed at the Cu K-edge to determine the evolution of the short-range structure of the less crystalline or amorphous copper phases which are not accessible by the *in situ* XRD measurements under reaction conditions. A principal component analysis of the Cu K-edge XANES spectra revealed that three primary components were necessary to reconstruct the experimental

TABLE 3

Change of Catalytic Activity Data (Conversion of Methanol, Selectivity to CO_2, Hydrogen Production Rate) Obtained in XRD and XAS Cells after Repeated Oxidation and Reduction Steps

Sample name[a]	Number of oxidation/ reduction cycles[b]	Cu crystallite size (Å)[a]	XRD cell			XAS cell		
			X_{MeOH} (%)	S_{CO_2} (%)	r_{H_2}[d] (μmol $H_2 \cdot g_{cat}^{-1} \cdot s^{-1}$)	X_{MeOH} (%)	S_{CO_2} (%)	r_{H_2}[d] (μmol $H_2 \cdot g_{cat}^{-1} \cdot s^{-1}$)
C70/30	0	76	25	75	483	25	54	145
	1	110	62	61	531	25	58	155
	2[c]	120	—	—	—	23	70	166
C60/40	0	100	51	37	470	20	48	133
	1	120	64	42	556	26	51	162
	2	130	62	42	535	27	53	176
C40/60	0	50	40	50	450	20	53	150
	1	70	44	80	620	24	53	160
	2	80	36	94	618	—	—	—
C30/70	0	—[c]	—	—		20	53	105
	1					24	53	146
C10/90	0	—	—	—		13	55	92
	1					14	62	92
	2					14	62	103

All samples were prepared according to the constant pH method and reduced under "dry" conditions. The data were obtained at 523 K with a flow of MeOH/H_2O (ratio ~ 4/1) in 120 ml/min (XRD cell) or 25 ml/min (XAS cell). Conversion and selectivity are given as initial values.

[a] Based on the Scherrer equation for the Cu (111) reflection.

[b] "0" denotes the fresh reduced catalyst, where "1" and "2" refer to first and second oxidation/reduction cycle, respectively.

[c] Second oxidation step not performed.

[d] Production rate of hydrogen per gram of catalyst per second.

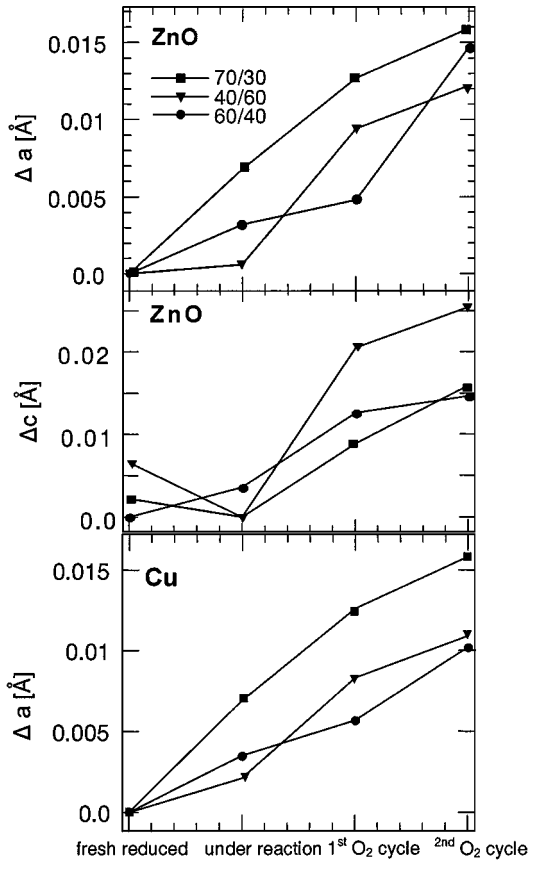

FIG. 6. Relative change of ZnO lattice parameters *a* and *c* (a) and Cu lattice parameter *a* (b) with respect to the values of the fresh reduced samples C70/30, C60/40, and C40/60 under methanol steam reforming, and after two successive oxygen addition cycles.

XANES spectra. Using target transformation three probable reference compounds (i.e., Cu, Cu(I) oxide, Cu(II) oxide) were identified. *In situ* XRD results have shown that Cu in the oxide precursor was CuO and that it was completely reduced by TPR to Cu. The "target-transformed" spectra showed a good match with the first experimental XANES spectrum (containing only CuO) and the last spectrum (containing only Cu) in the TPR run. However, the result of the transformation for the third component showed considerable deviations from the experimental spectra of commercially available pure Cu_2O. The poor match is probably due to the high crystallinity of the reference compound which may not reflect the local disorder (structural defects, decreased crystallinity and/or crystallite size) of the intermediately formed Cu(I) oxide. In order to account for the small crystallite sizes a reduction of the amplitude above the XANES edge of the experimental spectra resulted in an enhanced agreement with the transformed spectra. Hence, Cu(I) oxide is indeed an intermediate during TPR and the "target-transformed" spectrum was taken as a reference for Cu(I) oxide for the least-squares fits. The evolution of the phase composition during TPR of sample D70/30 under "dry" reduction conditions (2 vol% H_2 in 25 ml/min He, temperature ramp 448 K to 523 K at 5 K/min) is depicted in Fig. 7. It can be seen that the onset of reduction coincides with the evolution of H_2O and the uptake of H_2.

(b) Steam reforming of methanol. In Fig. 8 the Cu K-edge XANES spectra measured over a period of 20 min during oxygen addition to the feed at 523 K is presented. It can be seen that adding O_2 to the feed (15 vol%) results in an increase of the Cu K-pre-edge feature. This corresponds to the oxidation of Cu to form Cu(I) oxide and Cu(II) oxide. The evolution of the concentration of MeOH, H_2, H_2O, and CO_2 together with traces of methylformate and CO (lower part of the graph) during two oxygen addition cycles are depicted in Fig. 9. It can be seen that after each oxygen and subsequent reduction cycle the resulting catalyst produces an increased hydrogen concentration as compared to that obtained after the initial reduction in 5% H_2. The catalytic performance after two oxidation/reduction cycles of a number of samples is given in Table 3.

The evolution of the copper bulk phases (i.e., formation of CuO_{1-x} and re-reduction) and the corresponding gas-phase composition during one oxygen addition to the feed is shown in Fig. 10. It can be seen that oxygen in the feed leads to a rapid oxidation of the copper particles to Cu(I) oxide and Cu(II) oxide (with a ratio of ~3/1). After the O_2 has been switched off the catalyst is re-reduced in the feed, the CO and H_2O concentrations decrease, and the H_2 concentration increases. Apparently, reversible changes of the oxidation state of copper can be observed during oxygen cycles due to oxidation and subsequent re-reduction processes in the feed (see Fig. 8). A catalytic activity similar

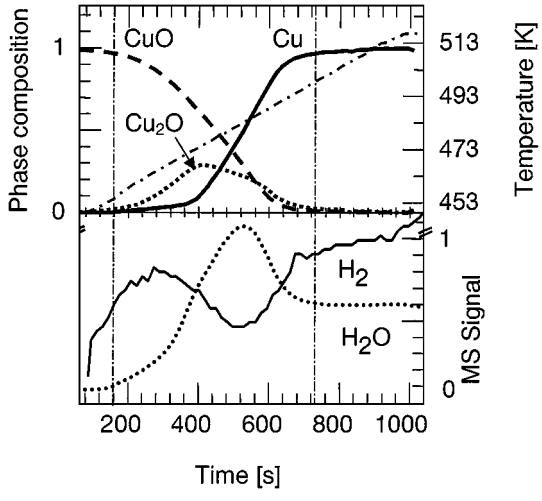

FIG. 7. Evolution of copper phase composition together with the MS signal of H_2O (dotted) and H_2 (solid) during TPR. The quantitative phase analysis is based on a least-squares fit of Cu K-edge XANES spectra of a CuO/ZnO sample (C70/30) during TPR in 8 vol% H_2 with 5 s/frame and a heating rate of 5 K/min using suitable reference spectra of Cu, Cu(I) oxide, and CuO as described in the text.

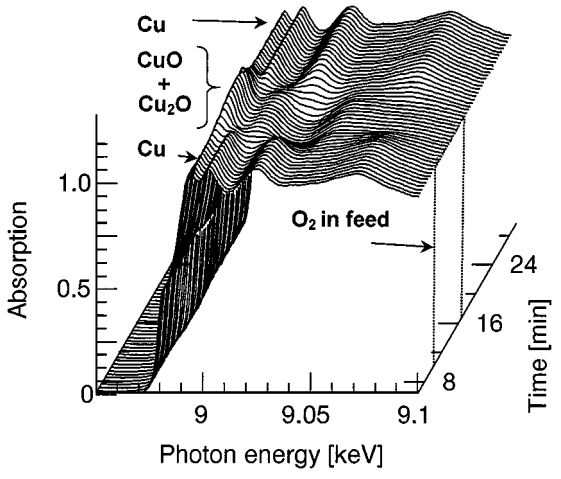

FIG. 8. Evolution of Cu K-edge XANES of CuO/ZnO at 523 K during oxygen addition to a methanol steam reforming feed (c(MeOH) ~6 vol%, c(H_2O) ~1.5 vol% in 25 ml/min He). Different Cu phases are indicated.

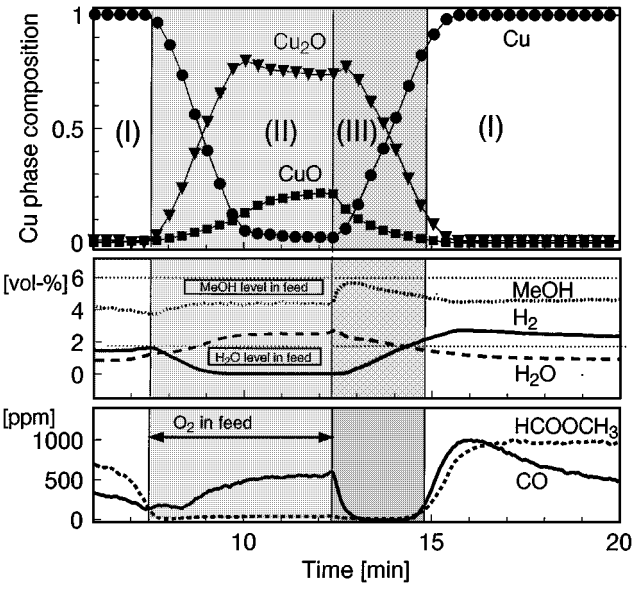

FIG. 10. Evolution of Cu phase composition during oxygen addition cycles into steam reforming feed at 523 K. Phase analysis was obtained from least-squares fit of reference spectra to the corresponding XANES spectra shown in Fig. 9. The two lower sections of the graph depict the evolution of the gas-phase in percent and ppm, respectively. Three transitions in bulk and gas-phase composition are marked: (I) copper metal during steam reforming, (II) oxidation to CuO_{1-x}, (III) re-reduction of CuO_{1-x} phases.

to that before the oxidation is regained after 4 min, at which time only copper metal can be detected.

The extended fine structure (EXAFS) of the experimental XAFS spectra measured under reaction conditions at the Cu K-edge and Zn K-edge was investigated to analyze changes in the short-range order structure of Cu and ZnO during repeated oxidation and re-reduction cycles at 523 K during methanol steam reforming. In Fig. 11 a refinement of a theoretical Cu EXAFS function to an experimental Cu FT($\chi(k)$) of sample C70/30 at 523 K under steam reforming conditions is depicted. Only the four most intense single-scattering paths in copper metal are displayed and a good agreement between experimental data and fit can be seen. The refined structural parameters are given in Table 4. During the fit the coordination numbers of Cu were kept constant to the values of bulk copper. This restriction is a reasonable assumption for the particle sizes investigated which have been shown by XRD to be larger than 80 Å. Therefore, size effects are assumed to play only a minor role in reduction of the amplitude

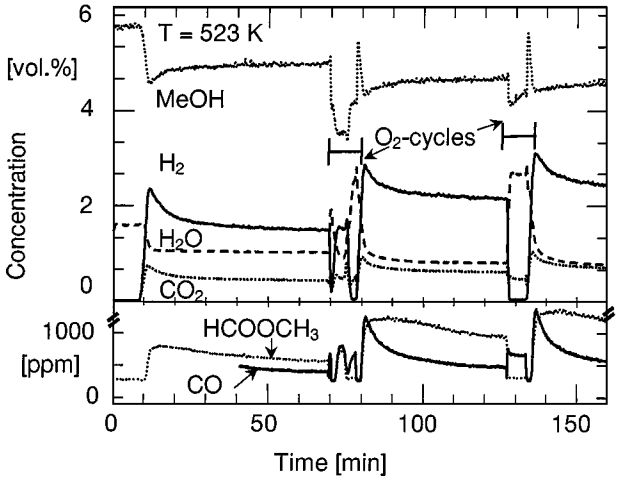

FIG. 9. Evolution of gas-phase composition (H_2, MeOH, CO_2, and H_2O) during oxygen addition to a methanol steam reforming feed in the *in situ* XAFS cell. Concentration of CO and $HCOOCH_3$ is shown in the bottom part of the graph (sample C60/40).

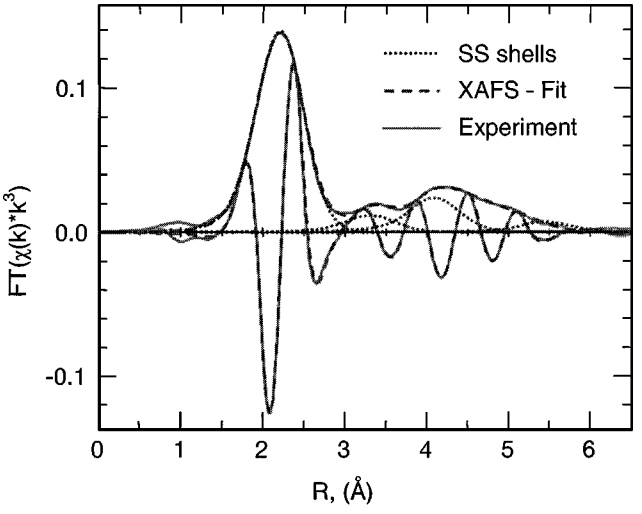

FIG. 11. Refinement of a sum of theoretical EXAFS function (dashed line) of Cu to an experimental FT($\chi(k)$) of sample C70/30 at 523 K after reduction in 2 vol% H_2. Only the four strongest single-scattering EXAFS functions are indicated (thin dark lines). Fitted parameters are found in Table 4.

TABLE 4

Structural Parameters of Cu/ZnO (C70/30) at 523 K under Methanol Steam Reforming Conditions (Fig. 11) Obtained from a Refinement of Theoretical EXAFS Functions Calculated for Cu Metal Cluster ($k = 2.0$ to 13.0 Å^{-1}, R = 1.5 to 6.0 Å, $N_{ind} = 32$, $N_{free} = 12$, 5 Single-Scattering Paths, and 14 Multiple Scattering Paths)

Shell	CN_{fixed}	R (Å)	ΔR_{foil} (Å)	σ^2 (Å^2)	w (%)
1. Cu–Cu	12	2.552	−0.004	0.0158	100
2. Cu–Cu	6	3.647	0.032	0.0246	9.567
3. Cu–Cu	24	4.437	0.01	0.0258	19.86
4. Cu–Cu	12	5.098	0.014	0.0963	0.443
5. Cu–Cu	24	5.826	0.111	0.030	6.187

Parameters refined are E_0(Cu) = 3.83 eV. The fit residual amounted to 2.8. Based on shells 1, 2, 3, and 5, an average lattice constant of a_0 = 3.6410 Å (Cu, $Fm3m$) was obtained.

in the FT($\chi(k)$) (40). Here the Debye–Waller (DW) factor is treated as a fitting parameter with coordination numbers fixed to those of the bulk metal. Hence, the Debye–Waller factor will be used to account for the apparent structural disorder in the copper crystallites and for the associated reduction in amplitude in the FT ($\chi(k)$). In the EXAFS analysis the Debye–Waller factors for the first, second, third, and fifth Cu–Cu shells are determined from a refinement of a theoretical EXAFS function to the experimental EXAFS functions of reduced binary samples measured at room temperature and at 523 K (shown in Fig. 12). For comparison, the DW factors obtained for a copper foil at room temperature are also given. It can be seen that the DW factors for the first three Cu–Cu shells for the samples at 523 K are higher than for those measured at room temperature. However, for samples C70/30 and C60/40 the DW factors of the fifth shell (5.7 Å) are about the same as those of the samples measured at room temperature. For samples C40/60 and C30/70 the DW factors are even lower at 523 K than at room temperature. The DW factors of the Cu foil are the lowest in all cases. After an oxidation addition cycle at 523 K the amplitude of the FT increases, indicating structural changes with respect to the fresh reduced catalyst. A smaller increase in FT($\chi(k)$) is noted after the second oxidation cycle. The variation of the Cu DW factors for the first, second, third, and fifth Cu–Cu distances obtained from fitting experimental spectra of samples C70/30 and C60/40 obtained under working conditions at 523 K for different oxidative treatments is displayed in Figs. 13a and 13b. An increasing Debye–Waller

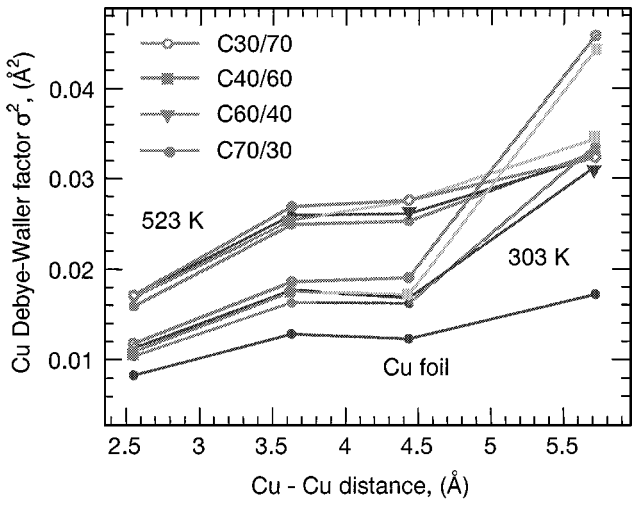

FIG. 12. Cu Debye–Waller (DW) factors, σ^2, for the first, second, third, and fifth Cu–Cu distances obtained from a refinement of a theoretical EXAFS function to experimental data for reduced samples C70/30, C60/40, C40/60, C30/70, and Cu foil obtained at 303 and 523 K under methanol steam reforming conditions.

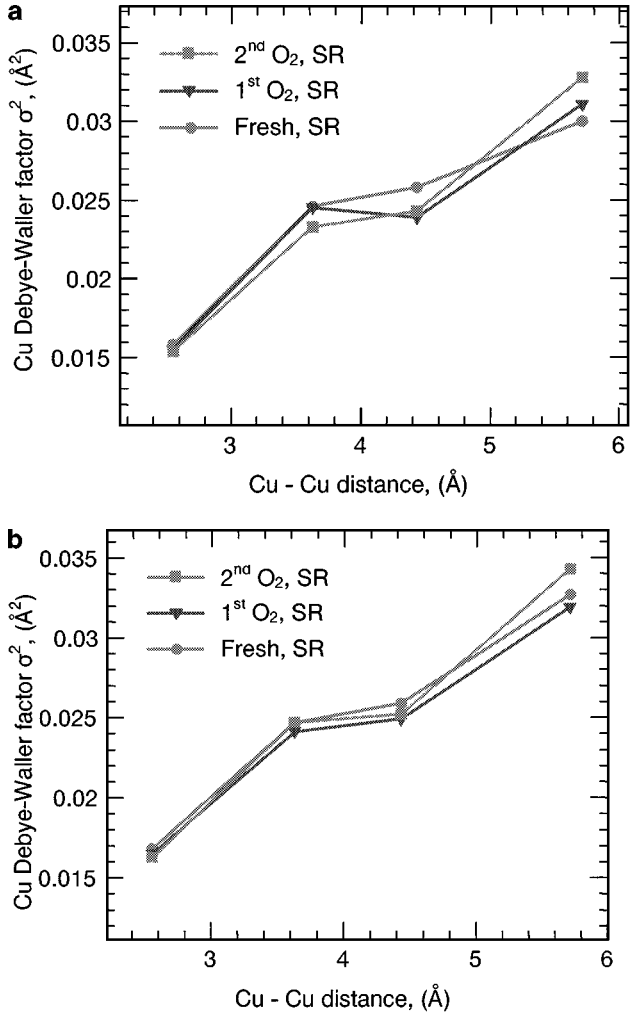

FIG. 13. Cu Debye–Waller (DW) factors, σ^2, for the first, second, third, and fifth Cu–Cu distances obtained from a refinement of a theoretical EXAFS function to experimental data for samples C70/30 (a) and C60/40 (b) obtained at 523 K during methanol steam reforming conditions after different pretreatment (fresh reduced) and after two subsequent oxidation and reduction steps (denoted as 1stO_2, SR and 2ndO_2, SR step).

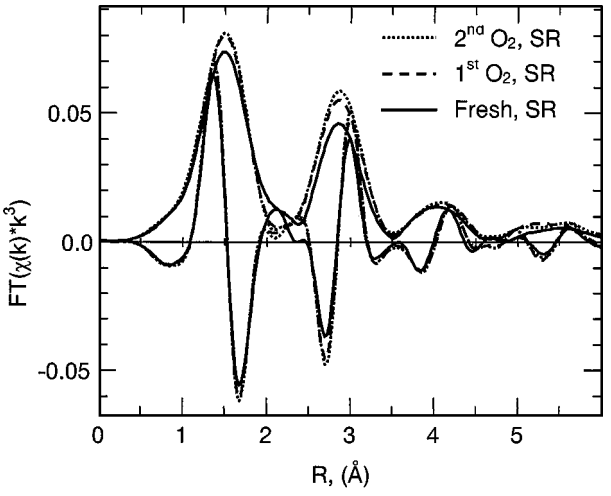

FIG. 14. Experimental Fourier-transformed Zn K-edge $\chi(k)$ (magnitude and imaginary part) of ZnO for sample C70/30 obtained at 523 K during methanol steam reforming reaction after different pretreatment (fresh reduced) and after two subsequent oxidation and reduction steps (denoted as 1st O_2, SR and 2nd O_2, SR step).

factor for the fifth Cu shell is detected for both samples after the second oxygen addition cycle. This effect seems to indicate an increasing medium range structural disorder in the copper particles with repeated oxygen addition cycles. Furthermore, changes in the local structural order of ZnO after oxidation/re-reduction cycles under reaction conditions were observed. In Fig. 14 the evolution of the experimental FT($\chi(k)$) of ZnO in sample C70/30 at 523 K during methanol steam reforming after initial reduction and after two oxidation/re-reduction cycles is depicted. A significant increase in amplitude of the FT($\chi(k)$) is clearly detectable with repeated O_2 addition cycles. Especially for the Zn–Zn distance at 2.8 Å a continuous increase can be seen. Higher shells also become more developed after repeated oxidation cycles. The observation of the increasing amplitude for both Cu and ZnO after oxidation and re-reduction implies that ZnO undergoes microstructural modification during oxidation/re-reduction cycles as well. To further elucidate the structural changes in the short-range order of ZnO after oxidation/re-reduction cycles, a refinement of theoretical EXAFS functions to the experimental spectra was performed. As an example, Fig. 15a shows the fit of a theoretical EXAFS function of ZnO to the experimental Zn K FT($\chi(k)$) of sample C70/30 under steam reforming conditions at 523 K. A significant deviation in amplitude and imaginary part of the FT($\chi(k)$) is observed between the experimental and the fitted spectra. However, by adding Zn–Cu shells for Zn atoms occupying Cu sites in Cu clusters a much better fit to the experimental FT is obtained as shown in Fig. 15b. This indicates that Zn in Cu clusters contributes significantly to the FT($\chi(k)$) of ZnO. By quantitative EXAFS fitting of a sum of the two phases (ZnO + Zn in Cu) it is possible to determine the amount of Zn in the Cu clusters. For sample C70/30 the contribution to the total amplitude from scattering paths of Zn in Cu for the fresh reduced sample under reaction conditions amounts to ∼10%. This amount diminishes to 5.1% after the first oxygen addition cycle and to 2.6% after the second cycle. By relating the contributions of scattering paths of Zn in Cu to the nominal Zn content of the samples, the concentration of Zn in Cu can be estimated. For the fresh reduced sample C70/30 4.3 mol% Zn was found to be dissolved in copper. After the first and second oxygen addition cycles the concentration of Zn in Cu was 2.2 and 1.1 mol%, respectively. For the sample C60/40 an amount of 2.4 mol% is dissolved in the Cu bulk of the fresh reduced sample, and this was reduced to 1.3 mol% and then 0.8 mol% after oxygen addition cycles.

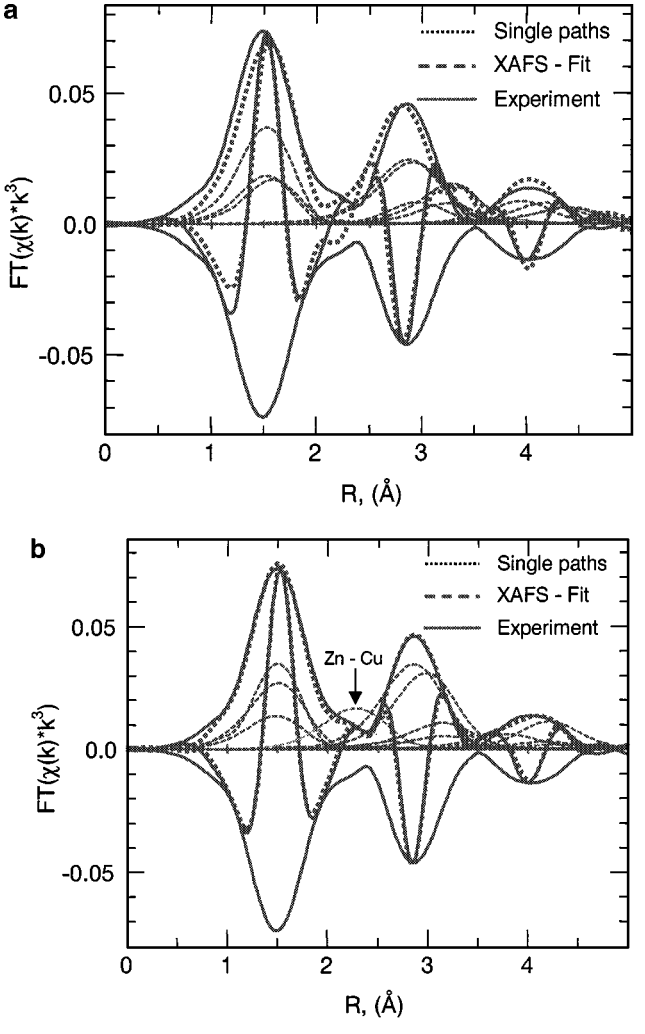

FIG. 15. Refinement of a theoretical EXAFS function (dotted line) of ZnO to an experimental FT($\chi(k)$) for the sample C70/30 after reduction in 2 vol% H_2 at 523 K: (a) pure ZnO and (b) assuming additional Zn–Cu shells by doping Zn into the Cu cluster.

DISCUSSION

(I) In Situ XRD

Dependence of reducibility on catalyst composition. The presence of water retards the reduction onset temperature (~10 K) and results in higher Cu crystallite sizes (Fig. 2). Although the Cu/Zn ratio has only a slight effect on the onset temperature samples with increasing Zn content have smaller Cu particle sizes. The decreasing slope of the temperature-dependent Cu crystallite size with increasing Zn content seen in Fig. 2 indicates that ZnO exerts a stabilizing influence on the Cu particles during temperature-programmed reduction. Figures 2a and 2b illustrate that during TPR the samples with the highest Zn concentration (samples with C40/60 and D40/60) exhibit only minor crystallite growth with increasing temperature, whereas the Cu clusters in samples with a higher Cu concentration tend to sinter more. Apparently, the tendency to sinter depends on the interaction with the ZnO matrix and the Cu/Zn ratio. These results confirm previous investigations concerning the function of ZnO to keep the Cu crystallites in a dispersed state and thus maintaining a high surface area as previously described by Chinchen *et al.* (41) and Spencer (42). The exceptions to the previously mentioned trends are the samples with 60 mol% Cu (C60/40 and D60/40) which show after reduction a Cu crystallite size that is 10 Å larger than that of the sample with 70 mol% Cu (C70/30 and D70/30). The dependence of the reduction rate of CuO on the precursor composition is in good agreement with previous results by Porta *et al.* (19) and Himelfarb *et al.* (17) from an *in situ* XRD study. We have shown that for Zn concentrations larger than 40 mol% the multiphasic composition of the hydroxycarbonate precursor shows a transition from the rosasite phase ($(Cu,Zn)_2(OH)_2CO_3$) to the aurichalcite phase ($(Cu,Zn)_5(OH)_6(CO_3)_2$) (27). The influence of the precursor structure which is apparently preserved in the calcined CuO/ZnO precursor can lead to an enhanced reduction rate through the beneficial interaction of various types of defects leading to an increased reactivity of the solid phase. Those defects may be introduced during calcination of the hydroxycarbonate precursor at mild decomposition temperatures affording a high density of defects in the oxide. Our results support previous findings by Shen *et al.* (26) and Porta *et al.* (19) on the effect of hydroxycarbonate precursor phases on the reducibility and Cu crystallite size. Furthermore, the nucleation process influences the reduction rate and it can be imagined that the interaction of the Cu metal nucleus with ZnO can lead to differences in the growth in three dimensions (19). In most cases the addition of water in "wet" reduction experiments caused a shift of the onset of reduction to higher temperatures (Table 1). The influence of water addition could be explained by both thermodynamic and kinetic effects. First, the water partial pressures employed for the "wet" TPR (~30 mbar) experiments dilutes the hydrogen and results in an increased formation temperature of the Cu phase due to the reduced reduction potential (43). Second, the inhibition of the reduction by additional water according to the law of mass action can occur as well. Third, there may be a retarding influence of water on the formation of Cu nuclei. This kinetic explanation has been previously discussed by Wimmer *et al.* for a TPR study of Fe_2O_3 particles under "wet" reduction conditions (44).

Effects of precursor preparation and reduction conditions on the catalytic performance. The influences of the Cu/Zn ratio and the reduction method on the selectivity in methanol steam reforming are discussed for both constant and decreasing pH sample preparation methods. Most samples exhibit an increasing selectivity with decreasing conversion. For instance, the selectivities of samples C50/50 and D50/50 increase from ~70% to ~80% while the conversion drops from 20 to 10%. The reduction procedure affects the catalytic selectivity more clearly than the pH during precipitation of the precursors. This dependence of the selectivity on the reduction conditions is in contrast to the TOF which seems to be unaffected by the reduction treatment of the samples. In addition, the elemental composition has a strong effect on the selectivity. An optimum composition in terms of selectivity is attained for a narrow range of 60–70 mol% Cu for the constant pH samples. This investigation of the selectivity of binary catalysts in methanol steam reforming supplements previous studies on the catalytic performance for binary Cu/Zn catalysts with different Cu/Zn ratios (13, 26). The most stable sample is C70/30 "wet" as it shows only a small variation in conversion and selectivity.

It is clear from Table 2 that there is no straightforward correlation of the production rate with the Cu surface area over the entire compositional range of the samples. In addition, it is found that although in most cases the "wet" reduction mode results in a higher copper surface area an enhanced production rate is not observed for those samples (e.g., samples D40/60, D50/50, and C70/30). In addition, in all cases, the D-series samples exhibit a higher activity for a given copper surface area than the C-series samples.

In order to relate differences in performance of the catalyst to effects originating from preparation parameters, the composition, and the reduction conditions, the production rate is normalized to the Cu metal surface area estimated from the copper XRD crystallite size. The initial TOF for H_2 is a function of the ZnO content (see Fig. 3). Comparing the TOF values (ranging from 0.2 to 1.3) to other studies which employ similar reaction conditions although with equimolar $MeOH/H_2O$ ratio it is found that they are of the same order of magnitude (13, 26). However, highest TOF values are reported by Shen *et al.* (26) for the pure copper sample whereas in our study the catalyst with 60 mol% Cu exhibits the highest intrinsic activity irrespective of preparation or reduction conditions. The TOF values

for catalysts with ZnO contents higher than 40 mol% Zn do not show the nearly linear increase in TOF with increasing Zn content seen in the samples with less Zn. For concentration >40 mol% Zn the TOF is independent of the Cu surface area and the values do not differ much as a function of preparation and reduction mode. Furthermore, catalysts prepared at decreasing pH displayed a higher overall TOF than samples prepared at constant pH. This indicates that the precipitation pH affects the activity of the copper in the final catalyst. The influence of the pH during preparation is only seemingly in contrast to the behavior of the selectivity, which showed no dependence on the pH during preparation, because for the determination of the TOF for H_2 all reactions affording hydrogen were taken into account. In addition, "wet" reduction leads to higher TOF values for the decreasing pH sample batch whereas "dry" reduced constant pH samples exhibit slightly higher TOF values. The significant deviations from a constant TOF as a function of the composition imply that the copper surface area alone cannot adequately account for the differences in intrinsic activity. The catalyst D60/40 is exceptional as the activity of a copper surface atom can be twice as high for a given elemental composition as that for the sample C60/40, indicating the influence of preparation parameters on the catalytic activity as a function of the pH during preparation (i.e., increased TOF) (Fig. 3).

The absence of a linear relationship between the copper surface area and the methanol steam reforming activity provides additional evidence that the methanol steam reforming reaction is "structure sensitive." This is in contrast to results by Shen *et al.* (26) who proposed that the production rate is associated with the surface of metallic Cu. A "structure sensitivity" was reported by Hadden *et al.* (45) for the water–gas shift reaction. They have shown that the specific activity is not directly correlated to the Cu metal surface area and concluded that preparation parameters determine to a large extent the activity for a given Cu surface area. In a recent publication by Peppley *et al.* a kinetic model for methanol steam reforming is presented (6). It was found that the methanol steam reforming reaction and the methanol decomposition to CO and hydrogen proceed on different active sites, although the rate-determining step (dehydrogenation of absorbed methoxy groups) is the same in both cases. Furthermore, it was shown that the active site responsible for the methanol steam reforming reaction is similar to the one responsible for the water–gas shift reaction. This type of site is thought to be formed *in situ* and incorporates the presence of Cu^{2+} aggregates stabilized by hydroxyl and carbonate groups (46).

The present work indicates that an additional microstructural parameter different from the Cu surface area is operative. This becomes more apparent in the catalytic experiments after oxidation/re-reduction cycles. *In situ* XRD afforded an increase in crystallite size after the oxygen addition cycle accompanied by an increase in conversion of methanol and selectivity to CO_2 (Table 3). The increase in crystallite size can reach up to ~90% (from 70 Å to 120 Å for the sample C70/30). The origin of this pronounced increase in Cu crystallite size after each oxidation cycle can be related to a structural rearrangement during oxidation and re-reduction (Fig. 4). Although the increase in Cu particle size results in a loss of Cu surface area, higher conversions and selectivities are observed (Table 3) after oxidation cycles. Combining the activity data for the oxidation cycles shown in Fig. 5 (sample C60/40) with the Cu crystallite size determined by *in situ* XRD an increase of the TOF as a function of oxidation cycle can be measured. After the first cycle the TOF increases from 1.1 to 1.5 and after the second cycle the TOF reaches 1.6 s^{-1}. Again, these observations are in contrast to the simplified correlation of the catalytic activity with the Cu surface area and, hence, the crystallite size (26). A lattice parameter determination by *in situ* XRD yielded a continuous increase of the copper lattice parameter and the ZnO lattice parameters *a* and *c* under methanol steam reforming conditions and with each oxygen addition cycle (Fig. 6). The evolution of the lattice parameters may originate from the influence of the Cu/ZnO interface which may increase after each oxygen addition cycle, increasing the effect of the misfit of the two lattices (see below, XAS discussion). Using the Voigt method (47) it is found that in addition to size effects the broadening of the Cu (111) diffraction line is also caused by microstrain in the Cu bulk. For the sample D60/40 a Cu crystallite size of 90 Å was determined while the extent of strain amounted to 0.7%. After oxidative treatments and growth of the copper crystallites (increase in size to 102 Å) the strain contribution to the peak broadening (0.7%) was unchanged, indicating that there was no accompanying annealing of defects.

Apparently, the reoxidation experiments in the XRD cell show that a high Cu surface area is a prerequisite for an active Cu/ZnO catalyst. However, additional microstructural parameters need to be considered to account for the activity and selectivity observed. Further evidence for bulk structural changes under reaction conditions were gained from the *in situ* XAFS experiments.

(II) In Situ XAFS

Activation of the CuO/ZnO catalysts—TPR. Time-resolved XANES experiments at the Cu K-edge indicate that Cu(I) oxide is an intermediate of the reduction of the CuO/ZnO systems studied (Fig. 7a). In addition, these experiments afforded the evolution of the three phases CuO, Cu, and Cu(I) oxide during temperature-programmed reduction of CuO/ZnO (Fig. 7) not accessible by conventional TPR studies. Previously, features in the TPR spectra of CuO/ZnO system were attributed to different degrees of dispersion of the CuO without taking possible intermediates during the reduction processes into account (12).

Compared to *in situ* XRD results where the detection of copper metal requires a certain minimum crystallite size which in TPR causing a delay in the appearance of copper metal after detection of the evolution of water, *in situ* XAS can afford complementary information on the early stage of reduction. Apparently, the reducibility of the CuO/ZnO systems (Cu nuclei formation during reduction) depends not only on the Cu/Zn ratio in the catalyst as has been reported before (12) but also on the preparation conditions of the hydroxycarbonate precursor. This supports previous findings on the influence of the preparation method on the reduction process by Fierro *et al.* (14) and Himelfarb *et al.* (17).

Steam reforming of methanol. Time-resolved *in situ* XAFS measurement were performed to correlate different copper phases with catalytic activity during oxygen addition cycles to the methanol steam reforming feed (Figs. 8 and 9). The changes in Cu phase composition and the evolution of the gas phase for one oxygen addition cycle are shown in Fig. 10. After the addition of oxygen, Cu(I) and Cu(II) oxide constitute the major copper bulk phases. In regime III (Fig. 10) copper metal is formed again and its formation is accompanied by an increasing hydrogen production but no CO or methyl formate is formed in this period. This could imply that the methanol dehydrogenation reaction is favored over Cu in a positive oxidation state. The formation of CO and methyl formate (ppm levels) originating from methanol steam reforming is observed only after the concentration of metallic copper in the bulk phase exceeds 80 wt% (regime III to I in Fig. 10). The maximum concentration of CO and methyl formate (1000 ppm) coincides with the complete reduction of the copper phases to Cu metal. Our observation of both methyl formate ($HCOOCH_3$) and CO in regime I (Fig. 10) supports the sequence of reaction steps involving dehydrogenation and methylformate formation. During subsequent methanol steam reforming, the CO level is continuously decreasing whereas the concentration of methyl formate remains constant. In this regime (I in Fig. 10) methanol steam reforming appears to be the predominant reaction. It can be concluded that the changes of bulk phase and gaseous product composition observed during oxygen addition cycles permit one to distinguish between different active states of copper operative in the Cu/ZnO system. The results support previous assumptions based on kinetic analysis of surface reactions that parallel reaction might occur on different active copper phases during methanol steam reforming (6, 8). Interestingly, the oxidation and reduction curves of Cu metal in the upper graph in Fig. 10 exhibit in both cases a similar sigmoidal shape for both solid-state processes, indicating similar rate-determining steps and reaction rates.

Implication of microstructural changes of Cu and ZnO on the catalytic activity. The existence of copper suboxides in the bulk during methanol steam reforming can be excluded within the detection limits of XAFS (∼1 wt%) in the XANES region. Furthermore, for the Cu edge EXAFS no Cu–O shells were distinguishable after applying the difference file technique. Nevertheless, the formation of mixed valence copper suboxides at the catalyst surface cannot be excluded. Surface oxygen atoms on copper (under methanol oxidation conditions) which are different from oxygen in well-defined copper oxides have recently been reported by Knop-Gericke *et al.* using surface-sensitive *in situ* XAS (48, 49).

In recent publications (50, 51) the dynamics of the Cu/ZnO system were ascribed to changes in the morphology of the Cu surface. Clausen *et al.* (50) observed using EXAFS dynamical changes of the system upon changing the reduction potential in the gaseous environment and ascribed them to changes in the surface morphology (wetting/nonwetting phenomena). They showed that by taking changes in surface area and morphology (i.e., formation of Cu(110) and Cu(100) surfaces with higher activity) into account a "dynamic" microkinetic model for the methanol synthesis reaction under different gas atmospheres could be deduced. Sakakini *et al.* (51) reported on surface morphology changes of a supported $Cu/ZnO/Al_2O_3$ catalyst using IR spectra of adsorbed CO. The copper surface termination and the activity for CO_2 decomposition showed a dependence on the reductive treatment after previous oxidation.

In the work presented here microstructural changes of Cu and ZnO upon oxygen addition cycles are correlated to methanol steam reforming activity. The EXAFS refinements to the experimental Cu and ZnO $\chi(k)$ gave ample evidence of the bulk structural interaction of both phases leading to the following structural changes (Figs. 11 and 15). The unusually high Debye–Waller factor of the fifth copper shell indicates a medium range structural disorder of the Cu/ZnO at room temperature (Fig. 12). This structural disorder may be caused by interaction at the Cu/ZnO interface assuming an expansion of the Cu lattice at the interface. An epitaxial orientation of the Cu (111) surface to the ZnO (001) surface has been found to exist in the Cu/ZnO system (52). Upon increasing the temperature to 523 K the copper lattice will expand more than the ZnO lattice because of the difference in the linear thermal expansion coefficients, α, of Cu ($\alpha_{Cu,500K} = 17.4 \times 10^{-6}\,K^{-1}$(53) and ZnO (perpendicular to the c-axis: $\alpha_{ZnO,500K} = 71.5 \times 10^{-7}\,K^{-1}$ (54)). At elevated temperature the thermal expansion of Cu results in a partial release of the lattice mismatch at the interface and, thus, in a reduction of structural disorder as indicated by the decreased or constant DW factors of the fifth Cu shell (Fig. 12).

In situ EXAFS measurements during oxygen addition cycles under methanol steam reforming conditions gave further evidence of microstructural changes in the Cu/ZnO samples (Fig. 14). The Cu Debye–Waller factors indicated that the medium range disorder for copper particles

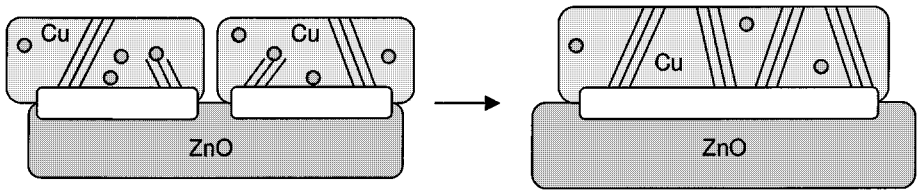

FIG. 16. Proposed schematic model for copper particles on a ZnO support after initial reduction (a) and after repeated oxygen addition cycles under methanol steam reforming conditions (b). The microstructural modifications upon oxidative treatment result in an increasing crystallite size and a larger interface area between Cu and ZnO. Moreover, the Cu clusters are depleted of Zn accompanied with larger domains of structural disorder (e.g., strain) in Cu (parallel lines).

increased with each oxidation/re-reduction cycle (see Fig. 13) while the copper crystallite size as detected by XRD increases after each oxygen addition cycle. After oxidation/re-reduction cycles the increase in medium range disorder is accompanied by a depletion of Zn incorporated in the Cu clusters (Figs. 14 and 15) (~4.3 mol% for sample C70/30 to 1.3 mol% after two cycles). The observed lattice expansion of <0.02 Å (Fig. 6) is below the limits for a reliable distance determination by EXAFS. The Zn atoms dissolved in Cu stem from the structural arrangement in the hydroxycarbonate precursor structure and maintain their position in the Cu matrix under the mild calcination (600 K) and reduction conditions (5 vol% H_2 at 523 K) used (39). Apparently, the amount of Zn dissolved in the copper clusters depends not only on the Cu/Zn ratio of the catalyst but also on the structure of the hydroxycarbonate precursor as indicated by the lower Zn concentration for Cu in the more Zn-rich C60/40 sample as compared to the C70/30 sample. The incorporation of Zn in Cu can be regarded as a modification of the copper surface leading to a modified reactivity as previously discussed by Nakamura *et al.* (55) for Cu/ZnO catalysts in methanol synthesis.

Moreover, substantial incorporation of Cu into the ZnO matrix (>1%) for Zn-rich catalysts as found by Klier *et al.* (56) can be excluded on the basis of their EXAFS results.

Taking this experimental evidence into account it seems reasonable to assume that the enhanced activity after oxidative treatment for methanol steam reforming is closely related to disorder and strain in Cu particles in an analogous manner as it was found for Cu/ZnO catalysts in methanol synthesis. Regarding the role of defects in copper we have recently reported (39) on the implication of the Cu lattice strain of copper clusters in the crystallite size regime 50–200 Å on the methanol synthesis activity. It is suggested that the microstrain modifies the Cu surface and thus contributes to an enhanced methanol synthesis activity (39). The structural defects of Cu were ascribed to the dissolution of Zn in Cu, incomplete reduction, or epitaxial orientation of Cu and ZnO. This concept seems to be transferable to the active copper phase in the methanol steam reforming reaction. Modified Cu surfaces were found to have a promotional effect on the methanol synthesis activity and it appears from our data that for methanol steam reforming a similar structural disorder of the copper bulk also results in a higher activity and selectivity. This is clearly shown by the increase of the TOF after each oxidation cycle, indicating a more active copper surface.

Model of microstructural changes of Cu and ZnO. The microstructural modifications detected by XAFS and XRD during oxygen addition cycles under working conditions can be summarized by the schematic model given in Fig. 16. The model depicts the structural rearrangement of Cu on ZnO for a freshly reduced catalyst (a) and a more active catalyst (b) after oxidation and subsequent reduction. For the freshly reduced catalyst the small copper particles are in interfacial contact with the supporting ZnO, possibly exhibiting an epitaxial orientation. The Cu crystallite size is only slightly lower than that of ZnO and the copper particles exhibit some structural disorder which may be caused by microstrain originating at the Cu/ZnO interface. Furthermore, a considerable amount of Zn (up to 4.3 mol%) is incorporated into the Cu clusters, occupying Cu lattice sites and forming a solid solution of Zn in Cu. After oxidation and subsequent reduction (Fig. 5) the crystallite sizes of Cu and ZnO increase, resulting in a reduced surface area which may also be accompanied by an increased interface area between Cu and ZnO. With the observed growth in crystallite size there is a decrease in the concentration of Zn in the Cu, and an *increase* in structural disorder in the Cu particles as indicated by the increasing Cu Debye–Waller factors for higher Cu–Cu shells. The partial segregation of Zn atoms out of the Cu lattice seems to increase interface interaction between Cu and ZnO. It is speculated that the Zn atoms incorporated in the Cu particles diminishes the effect of the Cu/ZnO interface on the copper particles and, therefore, the microstrain is not transmitted across the entire copper matrix, and does not modify the copper surface. Hence, after oxidation and re-reduction larger domains of distorted and strained copper are formed on the ZnO support. Much more than an inert support, ZnO appears to be a crucial component in modifying the microstructure (e.g., interface interaction, Zn incorporation in Cu particles), and thus the activity of the copper.

With respect to model systems for nanosized Cu/ZnO catalysts, in light of our findings, a suitable model system

needs to account for the strong support influence of ZnO on Cu and for Zn incorporated in the copper bulk.

CONCLUSION

Evolution of bulk phases of Cu/ZnO catalysts under reduction conditions was monitored by *in situ* XRD and XAFS revealing the following:

(a1) From time-resolved *in situ* XAFS experiments at the Cu K-edge, Cu(I) oxide was found to be an intermediate of the reduction of CuO/ZnO according to a two-step reduction process (CuO → Cu(I) oxide → Cu).

(a2) CuO/ZnO precursors which were less easily reduced (high reduction onset temperature) afforded Cu crystallites that are more selective in steam reforming of methanol. The use of "wet" reduction conditions, also resulting in a shift to higher onset of reduction temperatures, also produces catalysts exhibiting a higher selectivity.

Structural and catalytic properties were monitored during methanol steam reforming reaction by *in situ* XRD and XAFS and the following conclusions were drawn:

(b1) Completely reduced Cu clusters on ZnO constitute the active bulk phase for methanol steam reforming with no further oxidized Cu species detectable (<1%).

(b2) Upon repeated oxygen addition cycles, the catalyst exhibited an enhanced activity (i.e., increased TOF) and selectivity. It was shown by XRD and EXAFS that repeated oxygen addition cycles lead to a crystallite growth of both the copper and zinc oxide crystallites accompanied by a segregation of Zn out of the Cu bulk. However, the Debye–Waller factors for higher Cu–Cu shells suggest an increasing structural disorder (e.g., strain). The strain is thought to originate at the Cu/ZnO interface.

(b3) ZnO is not just a support but an integral part of the active Cu/ZnO catalyst. The bulk structure and, hence, the catalytically active surface is modified by the intimate Cu/ZnO interface.

(b4) The microstructural changes of copper and zinc correlate with increased methanol steam reforming activity and selectivity. This indicates that although a high Cu surface area is a prerequisite for catalytic activity, it does not account for the observed changes in activity and selectivity alone without taking bulk structural changes into account. We conclude that similar to methanol synthesis the enhanced activity in Cu/ZnO catalysts after oxidative treatment for methanol steam reforming is closely related to an increased disorder and microstrain in Cu particles.

In this study it was shown that for "real" Cu/ZnO catalysts solid-state transformation and interaction of the Cu and ZnO phases have a pronounced influence on the catalytic activity. Therefore, "ideal" Cu clusters fail to describe the structural imperfections observed and, hence, cannot be expected to be suitable model systems. Apparently, a suitable model system needs to account for both strong Cu/ZnO interface interactions and Zn incorporated in the copper bulk.

ACKNOWLEDGMENTS

The authors are grateful to Prof. Robert Schlögl for valuable discussions and continuous support. T.R. thanks the Deutsche Forschungsgemeinschaft "DFG" for financial support (Habilitationsstipendium). We acknowledge the Hamburger Synchrotron Radiation Laboratory, HASYLAB, for providing beamtime for this work.

REFERENCES

1. Takahashi, K., Takezawa, N., and Kobayashi, H., *Appl. Catal.* **2**, 363 (1982).
2. Amphlett, J. C., Evans, M. J., Mann, R. F., and Weir, R. D., *Can. J. Chem. Eng.* **63**, 605 (1985).
3. Peters, R., Dusterwald, H. G., and Hohlein, B., *J. Power Sources* **86**, 507 (2000).
4. Amphlett, J. C., Creber, K. A. M., Davies, J. M., Mann, R. F., Peppley, B. A., and Stokes, D. M., *Int J. Hydrogen Energy* **19**(2), 131 (1994).
5. Breen, J. P., Meunier, F. C., and Ross, J. R., *Chem. Commun.* 2247 (1999).
6. Peppley, B. A., Amphlett, J. C., Kearns, L. M., and Mann, R. F., *Appl. Catal. A* **179**, 21 (1999).
7. Jiang, C. J., Trimm, D. L., and Wainwright, M. S., *Appl. Catal. A* **93**, 245 (1993).
8. Peppley, B. A., Amphlett, J. C., Kearns, L. M., and Mann, R. F., *Appl. Catal. A* **179**, 31 (1999).
9. Clausen, B. S., Topsøe, H., and Frahm, R., *Adv. Catal.* **42**, 315 (1998).
10. Clausen, B. S., Steffensen, G., Fabius, B., Villadsen, J., Feidenshans'l, R., and Topsøe, H., *J. Catal.* **132**, 524 (1991).
11. Skrzypek, J., Sloczynski, J., and Ledakowicz, S., "Methanol synthesis." Pwn, Warsaw, 1994.
12. Fierro, G., Lo Jacono, M., Inversi, M., Porta, P., Lavecchia, R., and Cioci, F., *J. Catal.* **148**, 709 (1994).
13. Breen, J. P., and Ross, J. R. H., *Catal. Today* **51**, 521 (1999).
14. Fierro, G., Lo Jacono, M., Inversi, M., Porta, P., Cioci, F., and Lavecchia, R., *Appl. Catal. A* **137**, 327 (1996).
15. Ruggeri, O., Trifirò, F., and Vaccari, A., *J. Solid State Chem.* **42**, 120 (1982).
16. Plewa, J., and Skrzypek, J., *Chem. Eng. Sci.* **44**, 2817 (1989).
17. Himelfarb, P. B., Wawner, Jr., F. E., Bieser, Jr., A., and Vines, S. N., *J. Catal.* **83**, 469 (1983).
18. Vong, M. S. W., Sermon, P. A., and Grant, K., *Catal. Lett.* **4**, 15 (1990).
19. Porta, P., Dragone, R., Lo Jacono, M., Minelli, G., and Moretti, G., *Solid State Ionics* **32/33**, 1019 (1989).
20. Als-Nielsen, J., Grübel, G., and Clausen, B. S., *Nucl. Instrum. Methods* **97**, 522 (1995).
21. Reitz, T. L., Lee, P. L., Czaplewski, K. F., Lang, J. C., Poop, K. E., and Kung, H. H., *J. Catal.* **199**, 193 (2001).
22. Fernández-García, M., Rodríguez-Ramos, I., Ferreira-Aparicio, P., and Guerro-Ruiz, A., *J. Catal.* **178**, 253 (1998).
23. Grunwaldt, J.-D., Molenbroek, A. M., Topsøe, N.-Y., Topsøe, H., and Clausen, B. S., *J. Catal.* **194**, 452 (2000).
24. Idem, R. O., and Bakhshi, N. N., *Can. J. Chem. Eng.* **74**, 288 (1996).
25. Klier, K., *Adv. Catal.* **31**, 243 (1982).
26. Shen, G. C., Fujita, S., Matsumoto, S., and Takezawa, N., *J. Mol. Catal. A* **124**, 123 (1997).
27. Bems, B., Günter, M., Schur, M., and Schlögl, R., in preparation.

28. Ressler, T., Jentoft, R. E., Wienold, J., Günter, M. M., and Timpe, O., *J. Phys. Chem*. **104**, 6360 (2000).
29. Snyder, R. L., *in* "The Rietveld Method" (R. A. Young, Ed.), IUCr, Monographs on Crystallography 5. Oxford Univ. Press, London, 1993.
30. Kraus, W., and Nolze, G., PowderCell v2.2, Bundesanstalt für Materialprüfung, Berlin, 1999.
31. Designed by M. Hagelstein, T. Neisius, *et al.*, ESRF, France, in a collaborative effort with the Fritz-Haber-Institut, Berlin, Germany.
32. Ressler, T., *J. Synch. Radiat.* **5**, 118 (1998).
33. Ressler, T., Wong, J., Roos, J., and Smith, I. L., *Environ. Sci. Technol.* **34**, 950 (2000).
34. Rehr, J. J., Booth, C. H., Bridges, F., and Zabinsky, S. I., *Phys. Rev. B* **49**, 12347 (1994).
35. Rehr, J. J., Albers, R. C., and Zabinsky, S. I., *Phys. Rev. Lett.* **69**, 3397 (1992).
36. Bunker, G., *Nucl. Instrum. Methods* **207**, 437 (1983).
37. Ressler, T., Brock, S. L., Wong, J., and Suib, S. L., *J. Phys. Chem. B* **103**, 6407 (1999).
38. Anderson, J. R., and Pratt, K. C., "Introduction to characterization and testing of catalysts." Academic Press, New York, 1985.
39. Günter, M. M., Ressler, T., Bems, B., Büscher, C., Genger, T., Hinrichsen, O., Muhler, M., and Schlögl, R., *Catal. Lett.* **71**, 1–2 (2001).
40. Clausen, B. S., and Nørskov, J. K., *Topics Catal.* **10**, 221 (2000).
41. Chinchen, G. C., Denny, P. J., Jennings, J. R., Spencer, M. S., and Waugh, K. C., *Appl. Catal.* **36**, 1 (1988).
42. Spencer, M. S., *Topics Catal.* **8**, 259 (1999).
43. Gonzalez, J. C., Gonzalez, M. G., Laborde, M. A., and Moreno, N., *Appl. Catal.* **20**, 3 (1986).
44. Wimmer, O. J., Arnoldy, P., and Moulijn, J. A., *J. Phys. Chem*. **90**, 1331 (1986).
45. Hadden, R. A., Lambert, P. J., and Ranson, C., *Appl. Catal.* **122**, L1 (1995).
46. Andreev, A. A., Kalchev, M. G., Christov, G. D., and Andreeva, D. C., *Kinet. Katal.* **36**, 828 (1995).
47. Langford, J. I., *J. Appl. Crystallogr.* **11**, 10 (1978).
48. Knop-Gericke, A., Hävecker, M., Schedel-Niedrig, T., and Schlögl, R., *Catal. Lett.* **66**, 215 (2000).
49. Knop-Gericke, A., Hävecker, M., Schedel-Niedrig, T., and Schlögl. R., *Topics Catal.* **10**, 187 (2000).
50. Ovesen, C. V., Clausen, B. S., Schiøtz, P., Stoltze, P., Topsøe, H., and Nørskov, J. K., *J. Catal.* **168**, 133 (1997).
51. Sakakini, B. H., Tabatabaei, Watson, M. J., and Waugh, K. C., *J. Mol. Catal. A* **162**, 297 (2000).
52. Herman, R. G., Simmons, G. W., and Klier, K., *in* "Proceedings, 7th International Congress on Catalysis, Tokyo, 1980" (T. Seiyama and K. Tanabe, Eds.), p. 475. Elsevier, Amsterdam, 1981.
53. Uffelmann. L., *Philos. Mag.* **7**, 633 (1930).
54. Ibach, H., *Phys. Status Solidi* **33**, 257 (1969).
55. Nakamura, J., Nakamura, I., Uchijima, T., Wantanabe, T., and Fujitani, T., *Stud. Surf. Sci. Catal.* **101**, 1389 (1996).
56. Dominiquez, J. M., Simmons, G. W., and Klier, K., *J. Mol. Catal.* **20**, 369 (1983).